Low-Level Convergence Lines over Northeastern Australia. Part I: The North Australian Cloud Line

ROBERT GOLER,* MICHAEL J. REEDER,+ ROGER K. SMITH,* HARALD RICHTER,# SARAH ARNUP,+ TOM KEENAN,@ PETER MAY,@ AND JORG HACKER&

* *Meteorology Institute, University of Munich, Munich, Germany*

+ *Centre for Dynamical Meteorology and Oceanography, Monash University, Clayton, Australia*

Bureau of Meteorology Training Centre, Melbourne, Australia

@ *Bureau of Meteorology Research Centre, Melbourne, Australia*

& *Airborne Research Australia/Flinders University, Adelaide, Australia*

(Manuscript received 11 July 2005, in final form 12 February 2006)

ABSTRACT

Observations of dry-season north Australian cloud lines (NACLs) that form in the Gulf of Carpentaria region of northern Australia and the sea-breeze circulations that initiate them are described. The observations were made during the 2002 Gulf Lines Experiment (GLEX) and include measurements made by an instrumented research aircraft. The observations are compared with numerical simulations made from a two-dimensional cloud-scale model. Particular emphasis is placed on the interaction between the east coast and west coast sea breezes near the west coast of Cape York Peninsula. The sea breezes are highly asymmetric due to the low-level easterly synoptic flow over the peninsula. The west coast sea breeze is well defined with a sharp leading edge since the opposing flow limits its inland penetration, keeping it close to its source of cold air. In contrast, the east coast sea breeze is poorly defined since it is aided by the easterly flow and becomes highly modified by daytime convective mixing as it crosses over the peninsula. Both the observations and the numerical model show that, in the early morning hours, the mature NACL forms at the leading edge of a gravity current. The numerical model simulations show that this gravity current arises as a westward-moving land breeze from Cape York Peninsula. Convergence at the leading edge of this land breeze is accompanied by ascent, which when strong enough produces cloud. Observations show that the decay of the NACL is associated with a decline in the low-level convergence and a weakening of the ascent.

1. Introduction

The Gulf of Carpentaria region of northeastern Australia is well known for the different kinds of mesoscale cloud lines that frequently occur there (Drosdowsky and Holland 1987; Drosdowsky et al. 1989; see also Reeder and Smith 1998 for a review). A map of northern Australia with place names mentioned in the text is shown in Fig. 1. Often the cloud lines stretch across the entire length of the gulf from the extreme southeast to the far northwest, a distance of more than 500 km, and can occur nearly every day from September to November each year. The regular occurrence of these cloud lines makes this region meteorologically unique. Drosdowsky and Holland (1987) used the generic term, north Australian cloud line (NACL), for a variety of cloud lines commonly observed, although they identified three basic types of NACLs based on their shape and movement as observed by satellite. The three basic types are as follows:

- Type 1: long, thin cloud lines, either straight (Type 1a) or in the form of mesoscale arcs (Type 1b), generally comprising small cumuli, although isolated large cumuli or cumulonimbi and precipitation may occur also;
- Type 2: extensive areas of broken cloud, either stratiform or convective, up to 400 km across with a sharp leading edge similar to a Type-1 line;
- Type 3: overcast deep convective systems, such as

Corresponding author address: Dr. Robert Goler, Meteorological Institute, University of Munich, Theresienstr. 37, 80333 Munich, Germany.
E-mail: robert@meteo.physik.uni-muenchen.de

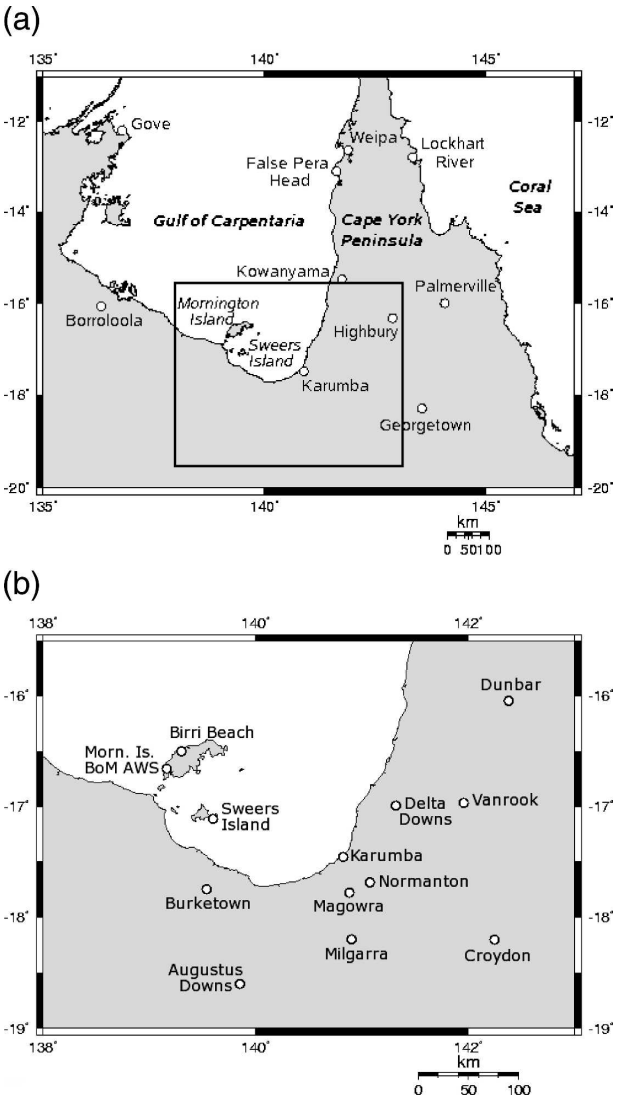

FIG. 1. Maps of (a) the Gulf of Carpentaria region and (b) a close-up of the southern gulf coast region, marked by the rectangle in (a). Other places mentioned in the text are marked.

tropical squall lines, comprising a sharp leading edge of deep convective cells and a trailing mesoscale stratiform anvil.

Type-1 and Type-2 lines are observed throughout the year but, according to Drosdowsky and Holland, they occur most frequently in the premonsoon months of September and October. Most Type-1 lines form near the west coast of Cape York Peninsula during the late afternoon and early evening and subsequently move westward across the Gulf of Carpentaria at speeds ranging from 4 to 15 m s^{-1}, with approximately 50% reaching Gove on the northwestern side of the gulf.

Three examples of NACL are shown in Fig. 2, which is a visible image from the Geostationary Meteorological Satellite (GMS) at 0632 EST.[1] A good example of a Type-1 NACL over the eastern part of the gulf is labeled 1 in this figure. During the dry season (April–October) the cloud lines that form in the gulf region are relatively shallow and generally do not produce rain but, during the transition and wet seasons (November–March), they may develop into thunderstorms with severe wind squalls and heavy rain showers. It is the latter type of cloud line that is of particular interest to forecasters because thunderstorms are intrinsically difficult to predict and, in this case, such storms can affect large regions of northern Australia, including the "Top End."

Another kind of cloud line is the well-known "morning glory," a series of low-level roll clouds that occur early in the morning at places around the southeastern part of the gulf and over the southwestern part of Cape York Peninsula (see, e.g., Smith 1988; Christie 1992; Reeder and Smith 1998). This particularly spectacular type of cloud line has been documented in a series of field experiments (Smith and Goodfield 1981; Clarke et al. 1981; Smith 1981, 1986, 1988; Smith and Morton 1984; Smith and Page 1985; Smith et al. 1982, 1986; Reeder et al. 1995; Menhofer et al. 1997a,b; Reeder and Christie 1998). Morning glories have also been observed in southern Australia (Clarke 1986) and elsewhere in the world [e.g., the United States (Haase and Smith 1984) and Germany (Hoinka and Smith 1988)]. In these cases, the morning glory was observed ahead of cold fronts or thunderstorm outflows, and its occurrence was not fixed to a particular geographical location as is the case for the morning glories in the gulf region. The regular occurrence of the morning glory around the Gulf of Carpentaria makes this an ideal region in which to study its development.

Interest in the morning glory stems from it being a wind shear hazard in the lower levels of the troposphere, which can be dangerous for aircraft taking off from or landing at airports (Doviak and Christie 1989). In addition, the vertical motion associated with the morning glory can be sufficient to initiate thunderstorms (Purdom 1976), which makes it important for weather forecasters to consider when forecasting convective development.

Figure 2 shows an extensive northwest–southeast oriented family of roll clouds (labeled 2) that had propagated from the northeast; such cloud lines are called "northeasterly morning glories." The image also shows a family of east–west oriented roll clouds (labeled 3), known as a "southerly morning glory," located inland

[1] EST = UTC + 10 h.

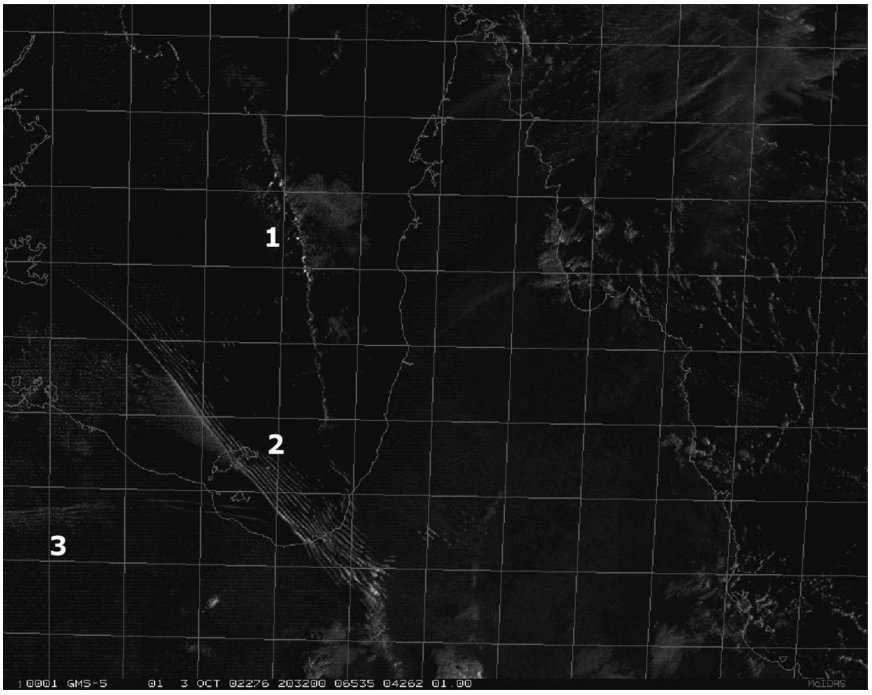

FIG. 2. GMS visible satellite image of the Gulf of Carpentaria region at 0632 EST 4 Oct (2032 UTC 3 Oct), which shows three different kinds of cloud lines: Type-1 NACL that lies over the eastern part of the Gulf of Carpentaria and is oriented roughly north–south, Type 2 represents a northeasterly morning glory located in the southern part of the gulf and oriented roughly northwest–southeast, and Type 3 represents a southerly morning glory that lies mostly south of the gulf and is oriented east–west.

from the gulf and to the west of the northeasterly morning glory. The latter clouds were generated south of the gulf region as a ridge extended across northern Queensland. The term NACL often includes most cloud lines that form in the gulf region, including northeasterly morning glories but not those moving from the south. However, the term will be reserved here for the westward-moving convective cloud lines only.

The NACL was the focus of a field experiment carried out from 20 October to 2 November 1986 as a preliminary to the Australian Monsoon Experiment (AMEX; Holland et al. 1986; Drosdowsky et al. 1989). The precursor to most of the NACLs observed during the experiment was the deep cumulonimbus convection that developed above the sea-breeze convergence on the west coast of Cape York Peninsula. Subsequently, this convection initiated a cloud line that moved westward and decayed during the evening. Goler (2005) showed, however, that NACLs can also occur without the initial deep convection, and it is the formation of these NACLs that is the focus of this paper.

The typical mature NACL observed during AMEX consisted of either a long, narrow line, or a series of large connected cloud arcs of active convection that extended 3–5 km deep and moved slightly faster than the maximum easterly wind. In the terminology of Drosdowsky and Holland (1987), these were Type-1 and -2 NACLs. The clouds sloped eastward with height (in the direction of the upper wind shear), precipitated, and produced strong, evaporatively driven downdrafts. This structure was similar to a shallow version of the squall line described by Moncrieff and Miller (1976), and the westward propagation seemed to result from downdrafts "scooping up" slower, moist boundary layer air into the line.

Most of the foregoing cloud lines, including the wet-season lines of thunderstorms and possibly the southerly morning glories, are believed to be associated with low-level convergence lines that form as part of the thermally driven mesoscale circulations in the gulf region. Numerical model calculations by Clarke (1984), Noonan and Smith (1986, 1987), Smith and Noonan (1998), Jackson et al. (2002), and Goler and Reeder (2004) indicate that, except in the case of southerly morning glories, the convergence lines are generated over Cape York Peninsula in association with the sea-breeze-induced circulations over the peninsula. This being the case, the lines may be largely predictable.

Some evidence for this possibility was provided in a preliminary study by Jackson et al. (2002), who examined the capability of the mesoscale version of the Australian Bureau of Meteorology Limited Area Prediction System (meso-LAPS) (Puri et al. 1998) to forecast low-level convergence lines corresponding with selected cloud lines observed in satellite imagery. Unfortunately, the temporal resolution of the surface data network in the region was inadequate to corroborate the predictions. For this reason, the Gulf Lines Experiment (GLEX) was organized in the late dry season (September–October) of 2002 to take measurements of temperature, mixing ratio, and winds in and around the west coast sea breeze and the cloud lines in order to verify the numerical model predictions and to determine the structure of the various types of cloud systems that constitute the NACL. The experiment was organized by the Bureau of Meteorology, Monash University, and the University of Munich with the specific aims (i) to study the sea-breeze structure and evolution prior to the generation of the convergence lines; (ii) to document the interaction between the sea breeze and convergence lines, including the subsequent evolution of the convergence line that results from such an interaction; and (iii) to validate the meso-LAPS simulations of the cloud lines that form during the "dry" season.

The present paper is the first of two reporting on the cloud lines and their associated convergence lines that were documented during GLEX. Part I focuses on the sea breezes and NACLs, while Part II, Smith et al. (2006), documents morning glory disturbances originating to the south of the gulf and moving northward. A third paper (Weinzierl et al. 2006, manuscript submitted to *Wea. Forecasting*) will examine the northeasterly morning glories observed and the ability of meso-LAPS to forecast all the convergence lines. Infrared satellite imagery showed that the NACLs that developed during GLEX were not preceded by deep convection, unlike those observed during AMEX, and that they formed just after local midnight. The relationship between the NACL and the sea-breeze convergence during the late afternoon over the peninsula is addressed here using a combination of observation and high-resolution numerical modeling.

The paper is structured as follows: section 2 briefly outlines the GLEX field experiment and the instruments available. This section also describes the configuration used to model some of the events. The structure and evolution of the sea breezes is reported in section 3. Section 4 examines two particular NACLs observed during GLEX for which the aircraft was available, while section 5 describes the formation of the NACL based on the model results from the two NACL case studies. Finally, section 6 presents the conclusions.

2. The field experiment and numerical model

a. Field experiment

The network of automatic weather stations (AWSs) installed and maintained by the University of Munich are marked in Fig. 1 along with the Bureau of Meteorology's operational AWSs. These instruments measured wind speed and direction, pressure, temperature, and humidity at intervals of 1–2 min. During the period from 7 to 20 October the Airborne Research Australia Cessna was operative, and the measurements of the NACL from this aircraft were central to the experiment. The instrumentation included rapid update temperature, humidity pressure, and wind measurements at a frequency of 5 Hz, providing a horizontal resolution of approximately 15 m. The lowest transect flown during the day was at 70 m above ground level. However, during the night the lowest flights possible were at 520 m over land and 300 m over water.

b. Cloud model

The numerical cloud-scale model used in the present study is described in detail by Clark (1977). In brief, the model is nonhydrostatic, anelastic, and includes a parameterization of subgrid-scale mixing (Lilly 1962; Smagorinsky 1963). For simplicity, all the cloud model calculations presented are two-dimensional and neglect the Coriolis effect, which is small in the region of interest. In these calculations the horizontal grid spacing is 200 m, and there are 60 unevenly spaced levels in the vertical with the lowest level at 2 m and the highest level at 15 km. The lowest 500 m of the domain contains 16 levels, and the uppermost 4 km (10 levels) of the domain incorporates a Rayleigh friction absorber. In each numerical experiment, the model domain is 700 km wide, comprising a strip of land 200 km wide located between a western body of water 400 km wide and an eastern body of water 100 km wide (see Fig. 3). This topography is a representative east–west slice near Weipa. The aerodynamic roughness length of the land is specified as $z_0 = 0.1$ m, and orography is not included in the model. The temperature of the eastern body of water is held constant at 299 K, while that of the western body is set at 300 K to represent the slightly higher sea surface temperatures (SSTs) of the Gulf of Carpentaria compared with the Coral Sea. These SST values are based on data from the Bureau of Meteorology Specialised Oceanographic Centre. The model configuration is kept as simple as possible to retain only the

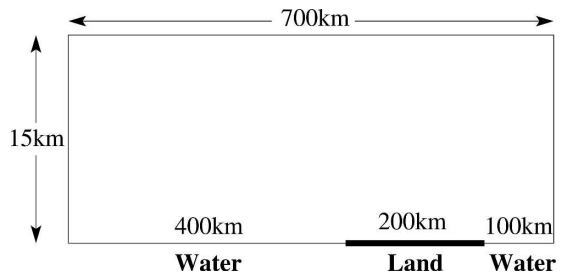

FIG. 3. Numerical model domain.

minimum number of processes considered to be essential to the formation of the cloud lines.

Each numerical experiment is initialized at model sunrise (0600 EST) using the 0900 EST sounding taken from Weipa (see Fig. 1) on the day prior to the development of the NACL (Weipa is the only sounding station available on Cape York Peninsula). The land is heated during the day according to a cosine profile with a maximum surface heat flux of 650 W m^{-2} at noon. During the night the surface cools at a constant rate of 40 W m^{-2}. These values were based on measurements of the surface energy budget over Cape York Peninsula by Tapper (1988).

3. Sea breezes over the peninsula on 7 October

The first aircraft mission flown during the experiment on 7 October included a transect across the entire Cape York Peninsula to examine the daytime structure of both the east and west coast sea breezes. Figure 4 shows the potential temperature, mixing ratio, and zonal velocity across the peninsula between 1515 and 1558 EST at a height of 70 m AGL. The orography of Cape York Peninsula is shown in Fig. 4d. Sharp jumps in the observed potential temperature, mixing ratio, and zonal velocity occur at about $x = 142.0°$E and mark the leading edge of the west coast sea breeze. In contrast, there is little evidence of the east coast sea-breeze front. Instead, east of $x = 142.4°$E there is a gradual decrease in potential temperature toward the east coast.

The observations of the east and west coast sea breezes presented here are similar to the numerical model calculations of sea breezes reported by Goler and Reeder (2004) in relation to the formation of the northeasterly morning glory. The asymmetry between the two sea breezes is due to the easterly flow that 1) restricts the inland movement of the west coast sea breeze, thus keeping it near to its source of cool air, and 2) aids the propagation of the east coast sea breeze across the land where the cooler air is subsequently mixed with the warmer land-based air by the convective eddies. A more detailed description of the sea-breeze asymmetry is presented in Goler and Reeder (2004).

The dashed lines in Fig. 4 are the equivalent profiles from a model simulation at 1530 EST. For the most part, the model reproduces the observations very well, especially given the idealized nature of the calculations. The main differences are that, at this time, the model places the west coast sea breeze about 16 km (0.15°) too far inland,[2] and it overestimates both the westerly wind within the west coast sea breeze (by a factor of 3) and the easterly wind ahead of the west coast sea breeze (by a factor of 2). The fact that this difference in zonal wind between that observed and that in the model decreases after sunset when boundary layer convection is reduced suggests a deficiency in the representation of convective mixing within the model (see later). When the model simulation was repeated with a 1 m s^{-1} easterly added to the initial flow, it was found that the position of the west coast sea breeze was shifted 0.1° westward, closer to the observed sea-breeze location. Such a modification to the initial velocity profile is within the observational uncertainty of the initial sounding. For this simulation and those that follow in later sections, the initial mixing ratio was reduced by 4 g kg^{-1} throughout the lowest 2 km of the troposphere to produce better agreement with the observed mixing ratio.

A vertical cross section from the model at 1530 EST is shown in Fig. 5a. The shading represents potential temperature, and the positions of the east and west coastlines are marked by the white dashed vertical lines. The west coast sea breeze is well defined but only about 400 m deep. Although the potential temperature gradient changes sign at about 142.3°E (Fig. 4), the easterly flow is highly modified by the daytime turbulent mixing over the peninsula, and consequently there is no well-defined east coast sea-breeze front.

Figure 6 shows the aircraft transects of potential temperature and zonal wind through the west coast sea breeze at a height of 110 m from 1751 to 1803 EST and at 450 m from 1833 to 1842 EST. Distance is measured eastward from the leading edge of the sea breeze. Over the course of these two time periods, the west coast sea breeze propagated 6 km (0.056°) eastward. Consequently, to aid the comparison, the latter transect has been shifted westward by this distance. Shown also in the figure are the corresponding traces from the model at 1800 and 1840 EST, respectively. The model data for the 1800 EST transect has been displaced westward by

[2] As noted later, the difference in position between the modeled west coast sea breeze and that observed reduces to 2.1 km by 1800 EST as the observed sea breeze propagates farther inland.

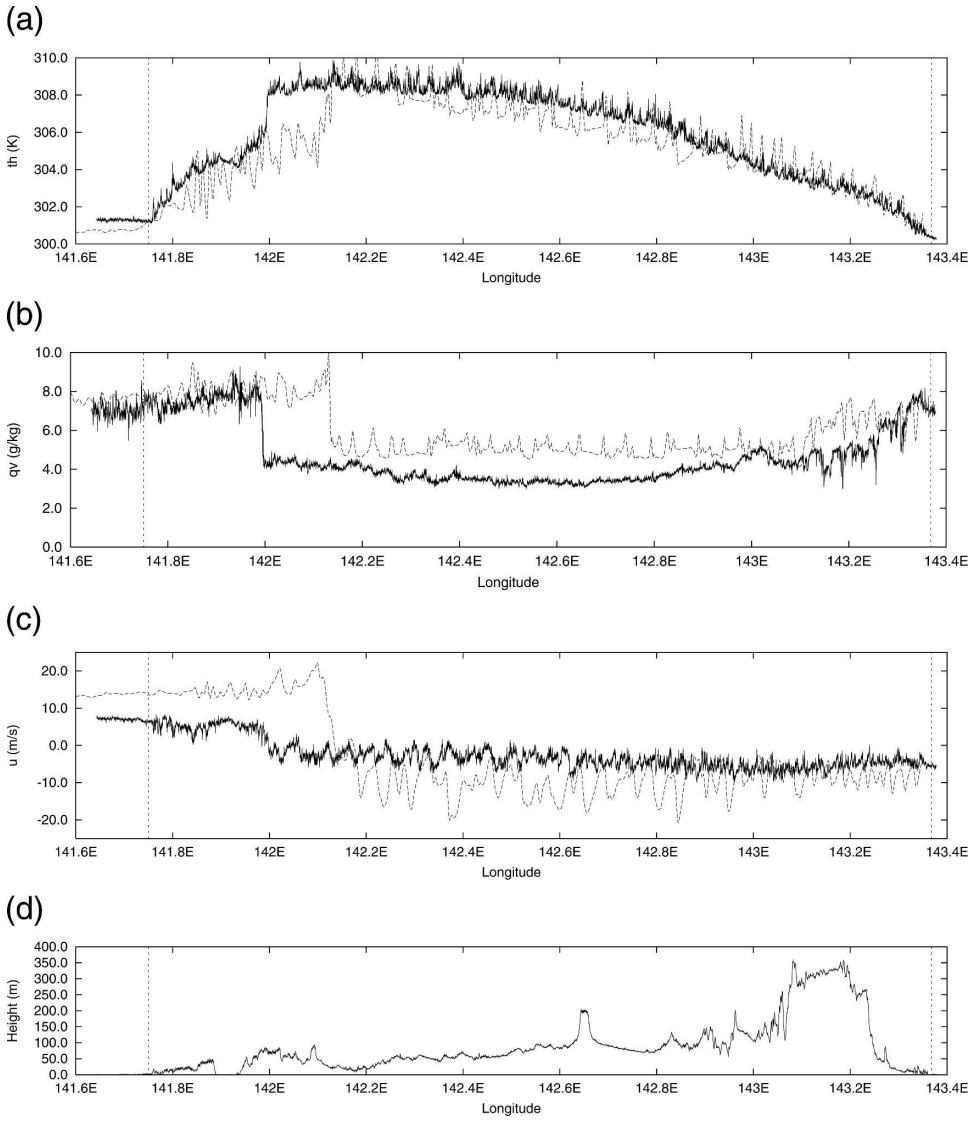

FIG. 4. Comparison between aircraft observations (solid lines) and numerical model data (dashed lines) at a height of 70 m AGL across Cape York Peninsula on 7 October: (a) potential temperature, (b) mixing ratio, and (c) ground-relative zonal wind. (d) The orography over Cape York Peninsula. The aircraft data were measured between 1515 and 1558 EST, and the equivalent instantaneous traces are taken from the model at 1530 EST. The vertical dotted lines in each plot mark the positions of the east and west coasts.

2.1 km (0.02°), and that for the 1840 EST transect eastward by 1.1 km (0.01°).

The model captures the structure of the west coast sea breeze well, although the potential temperature is, on the whole, too low in the lower trace. Furthermore, both the low-level westerly flow behind the sea breeze and the low-level easterly flow ahead of the west coast sea breeze is overestimated in the model by a factor of 2. A cross section at 1800 EST through the model simulation (Fig. 5b) shows the easterlies overriding the west coast sea breeze. These easterlies are cooler than the air in the convectively well-mixed layer that preceded the west coast sea breeze at 1530 EST (Fig. 5a). From this perspective, the leading edge of this cooler easterly flow might be characterized as the arrival of the east coast sea breeze.

The aircraft transect at 330 m (Fig. 6) can be interpreted more clearly with the help of the vertical cross section of the west coast sea breeze in the model shown in Fig. 5c. The white horizontal line shows the flight transect at the height of 330 m, which passes through the upper section of the cold air of the west coast sea

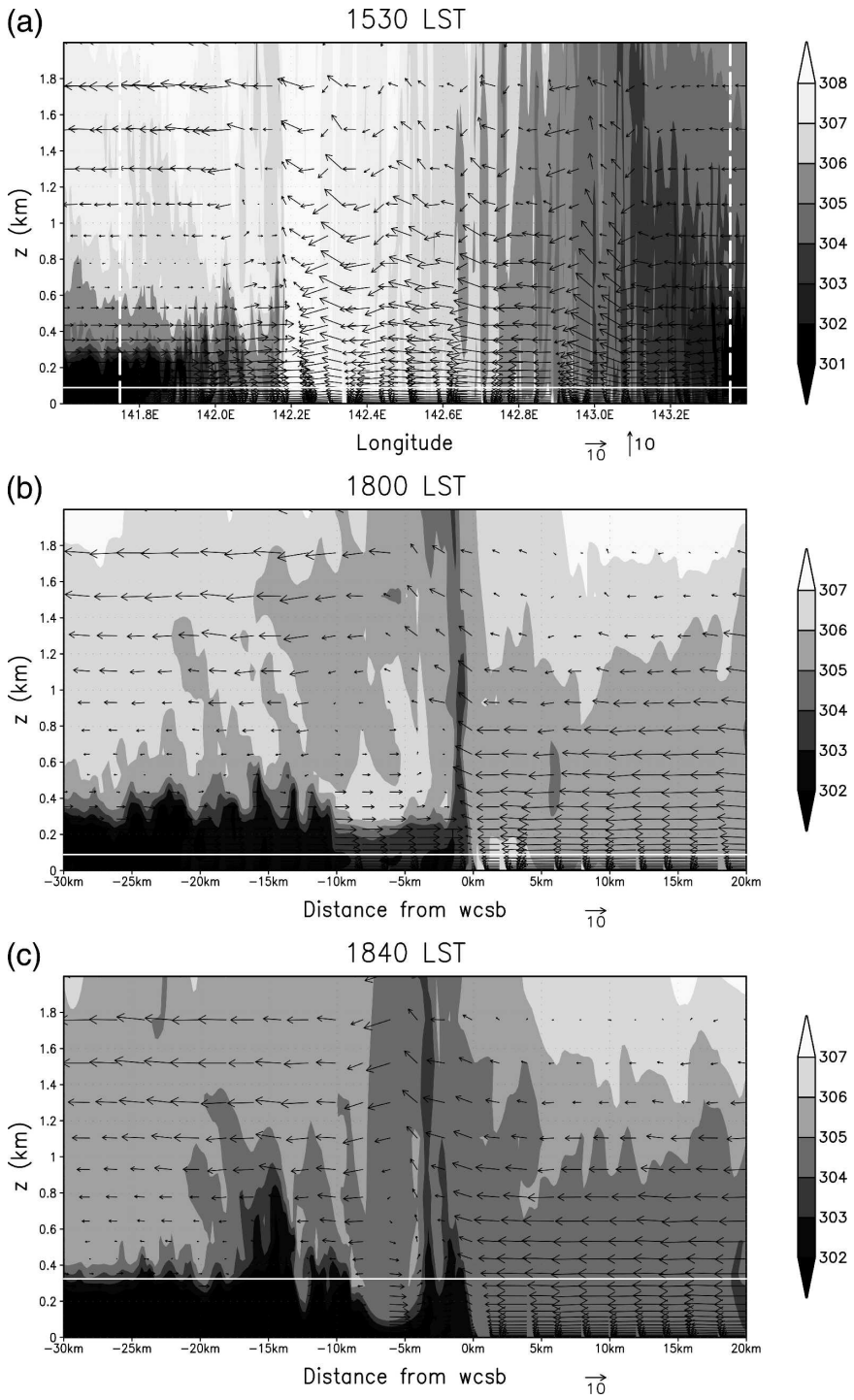

FIG. 5. Sea breeze on 7 October: Cross section of wind vectors and potential temperature (K) through the modeled sea breeze at (a) 1530, (b) 1800, and (c) 1840 EST. Potential temperature is shaded. The white horizontal line marks the flight transect at that time (see text for more details). The west and east coasts are marked in (a) by the vertical white lines. Velocity vectors are plotted relative to the ground at every 4 km in the horizontal in (a) and at every 1.4 km in the horizontal in (b) and (c). The vector scale in (b) and (c) applies to both the horizontal and vertical directions.

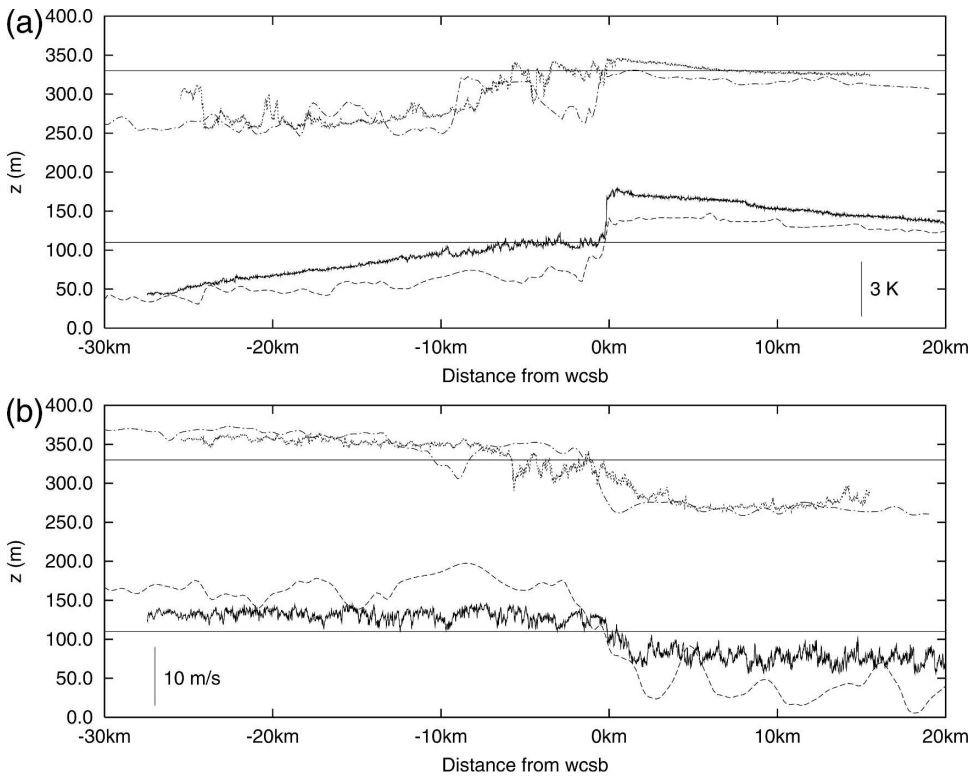

FIG. 6. Sea breeze on 7 October: Transect of (a) potential temperature and (b) zonal wind measured by the aircraft (solid lines) at a height of 110 m between 1751 and 1803 EST and at a height of 330 m between 1833 and 1842 EST. The equivalent instantaneous traces taken from the model are shown by the dashed lines at 1800 (110 m) and at 1840 EST (330 m). Distance is measured east from the leading edge of the west coast sea breeze (wcsb). Note that the later transect has been displaced 6 km (0.056°) westward to account for the movement of the west coast sea breeze. Furthermore, the model trace for the early transect has been displaced westward by 2.1 km (0.02°), and eastward by 1.1 km (0.01°) in the second transect.

breeze. Ahead of the west coast sea breeze the traces of potential temperature and zonal velocity are relatively smooth as the turbulence decays in the east coast sea-breeze air. The west coast sea breeze lies west of $x = -10$ km, as the air is cool and the flow is westerly. A transition region between $-10\text{ km} < x < 0$ km develops because of the mixing that takes place as the east coast sea breeze overrides the west coast sea breeze (Fig. 5c), entraining warmer and drier air into the west coast sea breeze. It is found in the model that the west coast sea breeze gradually decays as the entrainment of warmer and drier air into it continues. The role of the decaying west coast sea breeze in the development of the NACL will be further elaborated in section 5.

4. NACL events observed during GLEX

Infrared satellite imagery indicated that each of the four NACLs investigated during GLEX were first visible between 2130 and 0200 EST on the following day, which is different than the cloud lines observed during the pre-AMEX experiment. Moreover, the NACLs observed during GLEX were much shallower than those during AMEX, the cloud depths being less than 1 km deep and lacking precipitation. Each NACL during GLEX decayed in the late part of the morning and did not move beyond the middle of the gulf. Only the two NACL events with the largest potential temperature jump across the cloud line as observed by the aircraft will be described here, those being the events on 18 and 20 October. Observations from the aircraft will be presented along with comparisons from the numerical model simulations. The model simulations will be used in the following section to describe the formation of the NACL.

a. NACL on 20 October

The aircraft mission on 20 October focused principally on the vertical structure of the NACL by flying back and forth across it at various heights. The features

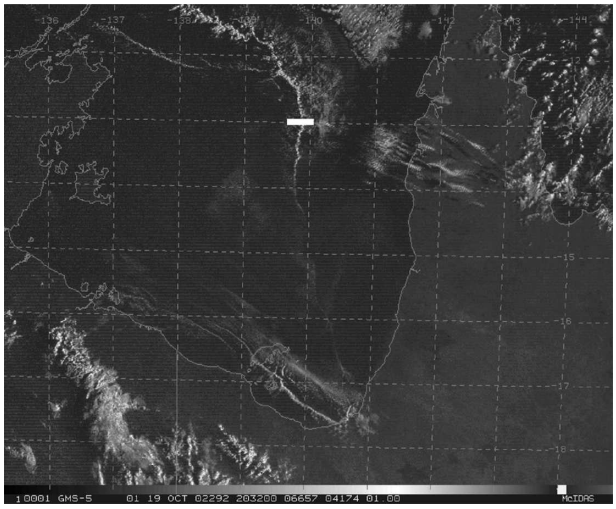

FIG. 7. NACL on 20 October: GMS visible satellite image of the gulf region at 0632 EST (2032 UTC) 19 October. The NACL is located west of Cape York Peninsula. The aircraft flight path is shown by the thick white line.

highlighted here were found to be common to each of the four NACLs observed during GLEX. Figure 7 shows a visible satellite image of the NACL just west of 140°E at 0632 EST, and the latitude of the flight transect is indicated by the white line.

The transects of potential temperature taken by the aircraft between 0646 and 0808 EST are shown in Fig. 8a, with horizontal distance measured eastward from the NACL. The sudden drop in potential temperature present in the lower transects coincides with the position of the NACL. Assuming that the cold air boundary does not slope appreciably with height, the speed of the NACL can be calculated from the movement of the potential temperature jump between the lowest three transects. In addition, the speed of the NACL can be calculated from its position in hourly GMS visible satellite images. Both methods yield a translation speed of -8.0 m s^{-1} during the time period when the aircraft observations were made, and this speed is used to refer all transects to a common origin, taken to be the position of the jump in potential temperature at 68 m.

The speed of the NACL can be compared to the theoretical speed of a gravity current within an environmental flow, which is given by Simpson and Britter (1980) as

$$c_g = 0.82\sqrt{g'H} + 0.61\overline{U}, \qquad (1)$$

where g' is the reduced gravity, H is the depth of the cool air, and $\overline{U}$ is the mean environmental wind ahead of the gravity current. Here, $g' = g\overline{\Delta\theta}/\overline{\theta}$, where $\overline{\Delta\theta}$ is the difference in potential temperature across the front of the gravity current, averaged over the depth of the gravity current, and $\overline{\theta}$ the potential temperature ahead of the gravity current, averaged through a depth H. Simpson and Britter obtained the coefficients in Eq. (1) from a sample of 20 observations of gravity currents in the atmosphere. Data from the aircraft observations shown in Fig. 8 can be used to evaluate Eq. (1). Using $H = 960$ m, the height at which the cooler air behind the NACL was observed,[3] $\overline{\Delta\theta} = 0.6$ K, $\overline{\theta} = 300$ K, and $\overline{U} = 7.0$ m s^{-1} gives a speed for the NACL of 7.9 m s^{-1}, which agrees with the observed speed of 8.0 m s^{-1}, supporting the idea that the NACL rides on the leading edge of a gravity current.

Figure 8b shows the equivalent plot of the zonal velocity relative to the NACL. The potential temperature fall behind (to the east of) the NACL coincides with an increase in easterly flow. The NACL-relative wind behind the NACL is a weak easterly, indicating that there is flow toward the leading edge of the cool air. At the 960-m level (not shown), the flow relative to the NACL is from front to rear. This wind structure also supports the idea that the NACL rides on the leading edge of a gravity current. The calculations of Thomsen and Smith (2006) indicate that the GLEX NACL event of 4 October had the nature of a gravity current.

Additionally, Fig. 8 shows the corresponding transects of potential temperature and zonal velocity from the model. For each transect the model data have been displaced 44 km (0.4°) eastward to remove the model phase error. The difference between the observed and modeled position of the NACL is due to the observed NACL having a slower translation speed of -6.2 m s^{-1} from 0030 to 0632 EST, as determined by its position in infrared satellite images. In the model, the NACL translation speed is approximately constant at -9.0 m s^{-1}. This difference of speed over the 6-h time period to 0632 EST would account for the NACL position in the model leading the observed by nearly a half degree.

The wind and potential temperature change at the position of the cloud line is reproduced well by the model at all levels. However, there are large deviations in potential temperature in the lowest two transects that are not evident in the observations. At all levels the model underestimates the observed potential temperature by as much as 1 K and above 200 m underestimates the temperature difference across the NACL. Generally below a height of 300 m, the model correctly represents the change in zonal wind across the NACL, although deviations of around 2 m s^{-1} exist.

[3] This was the highest transect flown in this event.

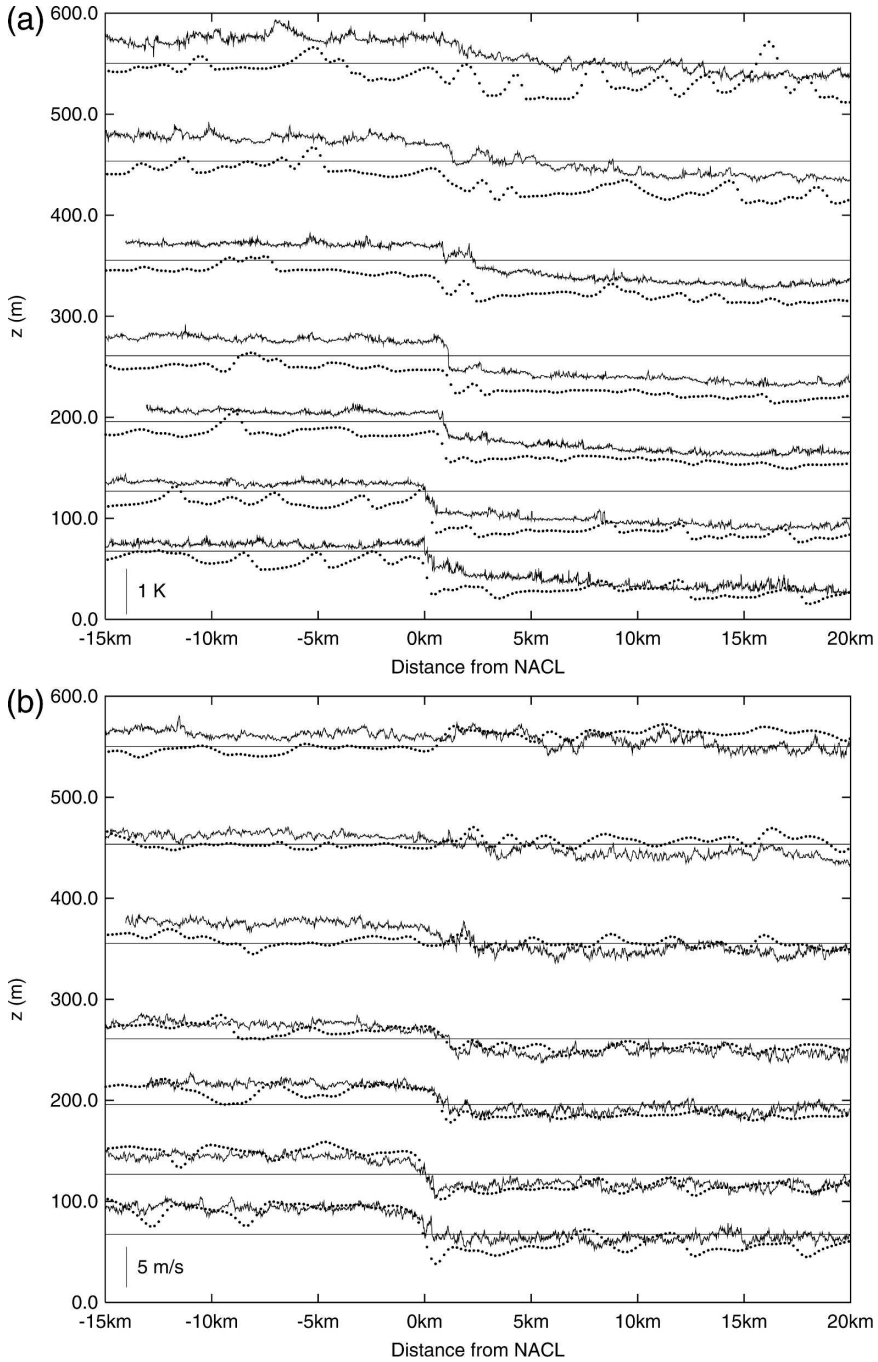

FIG. 8. NACL on 20 October: Measurements of (a) potential temperature and (b) zonal velocity relative to NACL made by the aircraft between 0646 and 0808 EST. The horizontal solid line represents $\theta = 300.5$ K in (a) and $u = -8.0$ m s^{-1} in (b). The corresponding transects in the model at the appropriate times are shown by the dotted lines.

b. NACL on 18 October

The aircraft mission on 18 October sought principally to document the temporal evolution of the cloud line. Figure 9 shows a visible satellite image at 0825 EST on 18 October (2225 UTC 17 October). The NACL is visible just to the west of Cape York Peninsula. The flight transect is marked on the satellite image by the white line and the position of Weipa by the white dot. Although not a focus of this paper, a northeasterly morn-

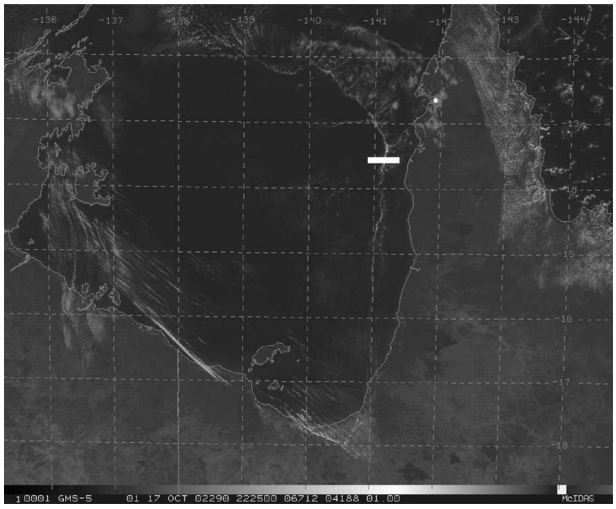

FIG. 9. NACL on 18 October: GMS visible satellite image of the gulf region at 0825 EST (2225 UTC) 17 October. The NACL is located immediately west of Cape York Peninsula. The flight path is shown by the white horizontal line. The location of Weipa is shown by the white circle.

ing glory is prominent across the southern part of the gulf.

Two transects through the NACL at a height of 70 m above sea level were made 108 min apart. During the first transect, the NACL was clearly identifiable as a near-continuous line of larger cumuli within the broad field of scattered cumuli. Figure 10 shows the potential temperature, the zonal wind relative to the NACL, and the mixing ratio from the first of these transects. In this figure the solid line represents the aircraft observations between 0822 and 0831 EST, while the dashed line represents the model results at 0830 EST. The model traces have been displaced eastward by 101 km (0.93°) to remove the model phase error. This large difference in position between the observed NACL and the modeled NACL can be partly explained by the flight path and the model cross section being different lines of latitude. Figure 9 shows that at the latitude of Weipa (model cross section) the NACL is about 0.5° farther to the west than at the latitude of the flight path. This means that the difference in position between the modeled NACL and that observed is about 44 km (0.4°).

The observed NACL coincides with the abrupt 0.6-K fall in potential temperature and 5 m s^{-1} change of the zonal velocity to a 2 m s^{-1} easterly. The initial fall in potential temperature in the model is about three times greater than that observed. However, farther behind the NACL, the difference between the modeled potential temperature and the observed potential temperature becomes smaller. The model's overestimate of the fall in potential temperature may be a result of insufficient mixing in the marine boundary layer in the model (see later). In addition, the cooler air immediately behind the NACL, and subsequent relatively higher pressure, may account for the translation speed of the NACL in the model being greater than that observed. Although the model overestimates the initial fall in potential temperature, the change in the zonal velocity across the NACL is reproduced well. The NACL-relative wind immediately behind the NACL is toward the leading edge of the cold air. However, about 22 km behind the NACL, the observed NACL-relative wind becomes westerly, while in the model westerly winds appear 40 km behind the NACL.

During the second transect at 70 m between 1007 and 1019 EST, the cloud line was noticeably shallower and hard to distinguish from the broad field of cumuli in which it was embedded. At this time the cloud base was at approximately 420 m. The potential temperature and relative zonal velocity from the two aircraft transects are compared in Fig. 11 with the later transect displaced eastward by 25 km to a common origin.

The potential temperature in the later transect is higher across the entire transect than in the earlier transect. The greatest rise in potential temperature occurs in the colder air east of the NACL. In this stable, cooler air the vertical mixing is confined to the layers adjacent to the surface because vertical motion is suppressed in the stable air. Ahead of the cloud line where the stability of the air is lower, there is less restraint on vertical motion. Therefore, the heating of the air column is distributed over a deeper layer, which results in a smaller temperature increase. In addition, the heat flux from the sea will be larger in the cold air since the difference between the air temperature and water temperature is larger. As a result, the drop in potential temperature across the NACL will be expected to become smaller with time unless some source of cool air is present, for example, evaporatively driven downdrafts that may accompany deeper, precipitating convection.

The vertical velocity at 258 m along the two transects is shown in Fig. 11c. In this figure, the second transect has been displaced eastward by 25 km, and +3.0 m s^{-1} has been added to the vertical velocity so that the change in vertical velocity between the two transects can be seen more clearly. In the second transect, the updraft at the leading edge is weaker than in the first transect, which is consistent with the decrease in the low-level convergence at the leading edge shown in Fig. 11b.

The modeled NACL described here weakened only slightly prior to reaching the edge of the computational domain 3 h later. When the model was rerun using a 1-K higher SST, the NACL did decay further, but its

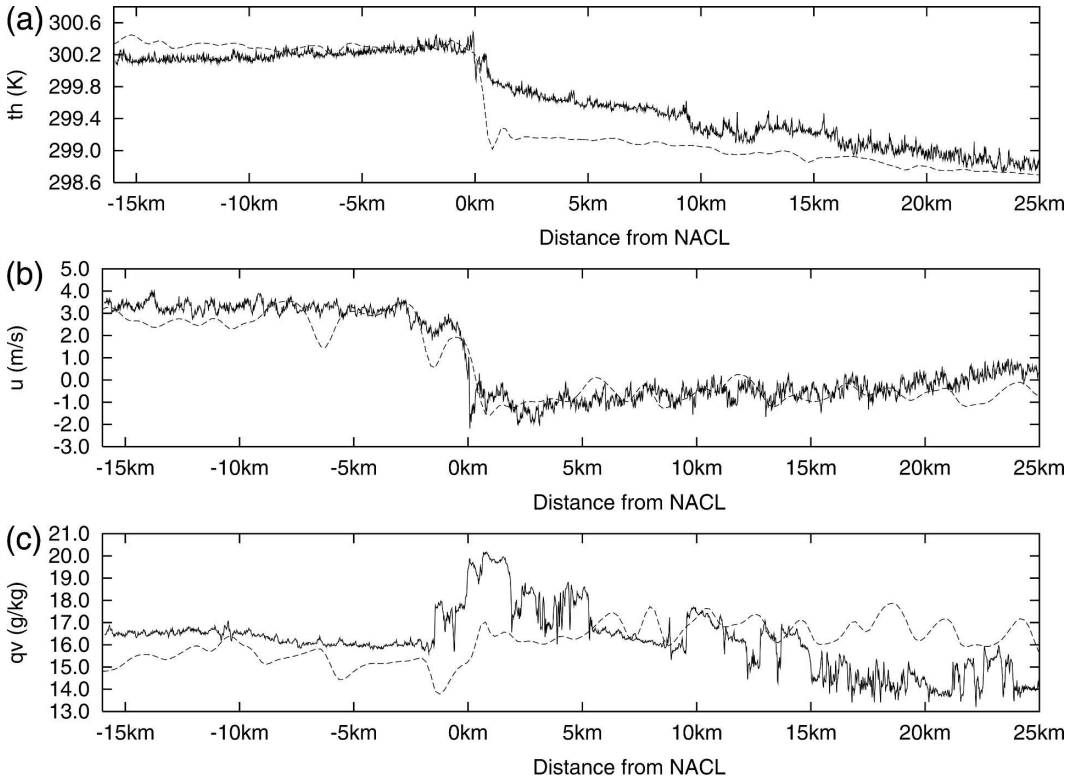

FIG. 10. NACL on 18 October: Transects of (a) potential temperature, (b) zonal wind relative to the NACL, and (c) mixing ratio, measured by the aircraft at a height of 70 m between 0822 and 0831 EST (solid lines), and the equivalent instantaneous traces taken from the cloud model at 0830 EST (dashed lines). The distance is measured eastward from the leading edge of the NACL. Note that the model traces have been displaced eastward by 101 km (0.93°) to make the comparison clearer.

position was 0.4° farther to the west of that in original simulation. Here the greater temperature difference between the cool air of the NACL and the air ahead of the NACL produced a faster translation speed.

Figure 12 shows the vertical profiles of potential temperature, mixing ratio, and zonal velocity taken by the aircraft about 54 km (0.5°) ahead of the cloud line and 54 km (0.5°) behind it, together with the equivalent profiles from the model. The sounding ahead of the NACL was taken between 0955 and 1006 EST (model data taken at 1000 EST), and the sounding behind was taken between 1114 and 1121 EST (model data taken at 1120 EST). The small difference in the low-level zonal flow between the sounding ahead of and behind the NACL in Fig. 12 is because the NACL weakened between the times of observation, as mentioned earlier. The sounding behind the NACL was taken some 80 min after the sounding ahead of the NACL.

The modeled potential temperature agrees well with the observed potential temperature, although above a height of 1.2 km the model is about 2 K cooler than observed. The easterly wind below 2.6 km in the model is at least 3 m s^{-1} stronger than observed. The model does not resolve the sharp change in mixing ratio at a height of 800 m and is drier than observed below this height. However, there is some doubt as to how representative the boundary layer sampled by the aircraft at that point in the descent is to the rest of the boundary layer. Figure 10c shows the mixing ratio at a height of 70 m observed between 0822 and 0831 EST. Ahead of the NACL it is less than 17 g kg^{-1}, while behind the NACL the observed mixing ratio is variable but not greater than 17 g kg^{-1}. Although the modeled mixing ratio (dashed line) does not exactly match the observed distribution and fails to capture the elevated values of mixing ratio at the cloud line, the magnitude of the mixing ratio is similar.

The translation speed of the observed NACL was 3.8 m s^{-1}. The data from the aircraft observations shown in Fig. 12 can be used to evaluate the speed from Eq. (1). Using $H = 400$ m for the observed depth of the cool air behind the NACL observed, $\overline{\Delta\theta} = 0.8$ K, $\overline{\theta} = 301$ K, and $\overline{U} = 1.8$ m s^{-1} gives a speed for the NACL of 3.9 m s^{-1}, which agrees with the observed speed, once again sup-

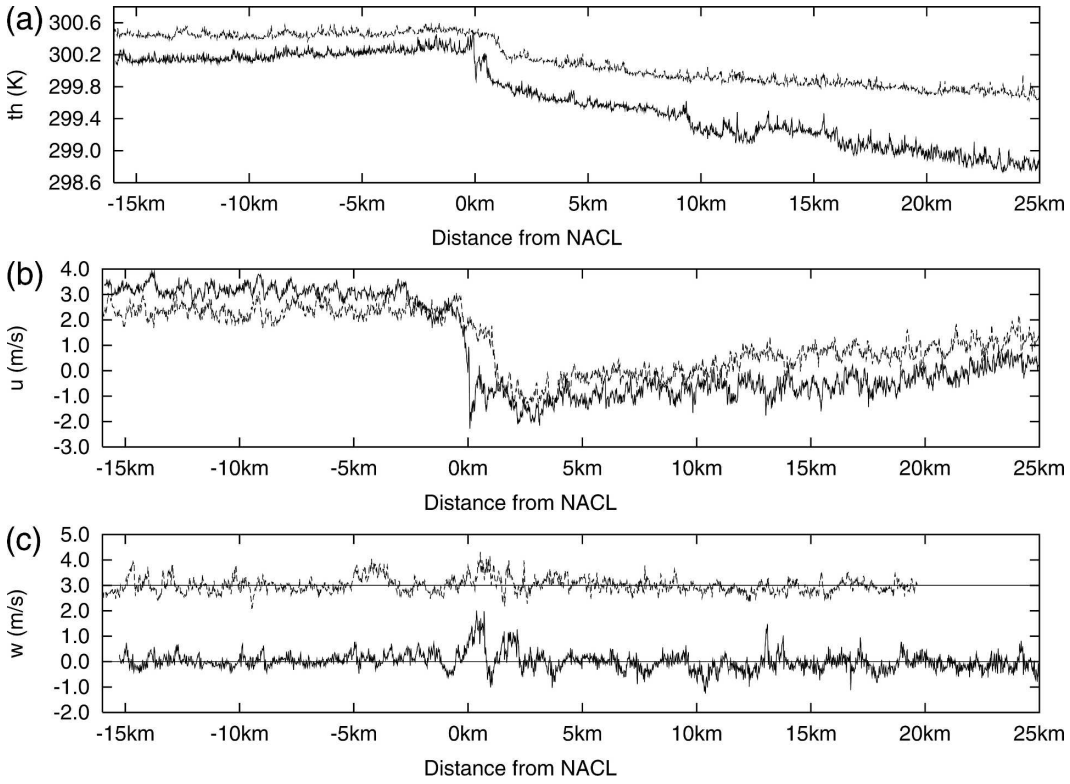

FIG. 11. NACL on 18 October: Two transects of (a) potential temperature at 70 m, (b) zonal wind relative to the NACL at 70 m, and (c) vertical velocity at 258 m measured by the aircraft. The solid lines are for the first transect from 0822 to 0831 EST, and the dashed lines are for the second transect from 1007 to 1019 EST. For ease of comparison, the second transect has been displaced eastward by 25 km and by $+3.0$ m s^{-1} in the case of the vertical velocity.

porting the idea that the NACL rides on the leading edge of a gravity current.

5. NACL development

Direct observations of the NACL in its developing stages were not possible during the experiment since it was unclear when it would develop. As the model was reasonably successful in capturing the observed characteristics of the two NACLs and the sea breezes in this study, we examine the mechanism by which the NACL forms in the model. Since the generation mechanism of the two NACL cases presented here is the same, the development will be described in general terms, utilizing model data from both cases to highlight specific points.

The east and west coast sea breezes develop during the day over the peninsula as in the 7 October case. The west coast sea breeze has a depth of about 500 m and is marked by a sharp drop in potential temperature and an increase in westerly zonal wind at its leading edge, while the east coast sea breeze is deeper and warmer with a more gradual change in potential temperature. The initial passage of the east coast sea breeze over the west coast sea breeze occurs at about 1800 EST. Progressively cooler air within the east coast sea breeze (see Fig. 4a), which is still warmer than the west coast sea-breeze air, flows over the west coast sea breeze. With time the sharp vertical gradient of potential temperature across the top of the west coast sea breeze is eroded. Figure 13 shows the vertical profile of potential temperature and zonal velocity from the model at a position of approximately 50 km west of Weipa for the 18 October NACL case at 1800 EST (solid line) and at 0000 EST (dashed line). The developing NACL passes this location at 0040 EST. The earlier sounding shows the cool air of the west coast sea breeze with strong westerly low-level flow. In the later sounding, a deep neutrally stratified layer of cool air has replaced the shallow layer of cold air.

The later sounding shows a weak easterly flow below 800 m compared with the strong westerly flow present earlier on. The reduction in the westerly flow is due to

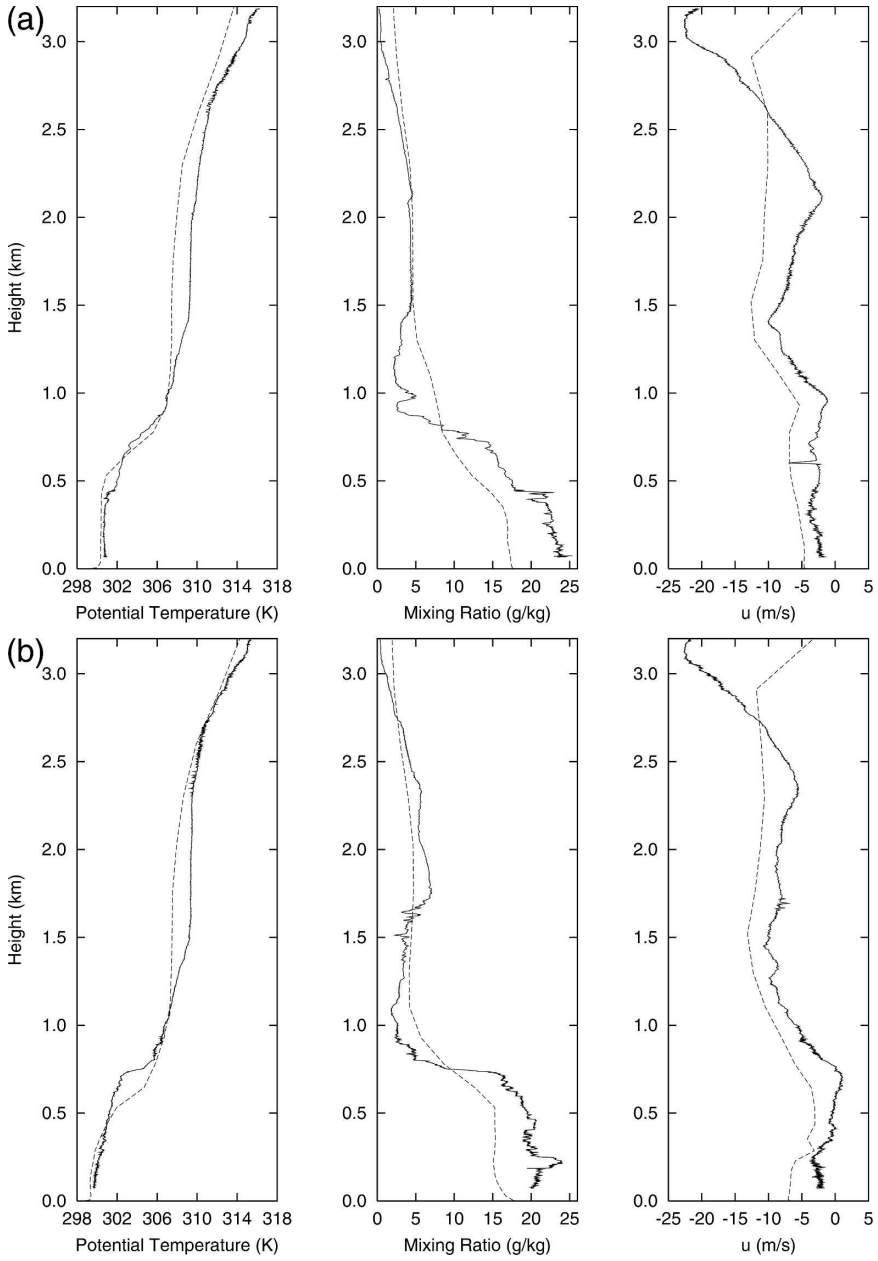

FIG. 12. NACL on 18 October: Vertical profiles of potential temperature, mixing ratio, and zonal velocity taken approximately (a) 54 km ahead of and (b) 54 km behind the NACL. Aircraft observations (solid line) and numerical model (dashed line).

the weakening, and eventual reversal, of the horizontal temperature gradient between the gulf and the land after sunset. Figure 14a shows a Hovmöller plot of the surface potential temperature shaded across the model domain from model initialization (0600 EST) to the end of the model run. From 0600 to 2000 EST, the air over the land is warmer than that over the gulf. After about 1800 EST the west coast sea breeze begins to warm and the air over the land cools, in part due to the advection of cooler air from the east and also from nocturnal radiative cooling.[4] Once the air over the land becomes cooler than the air over the gulf, the cool air propagates westward as a land breeze. The boundary of this land breeze is seen more clearly as a sharp increase in the

[4] There is no nocturnal cooling imposed over the water in the model.

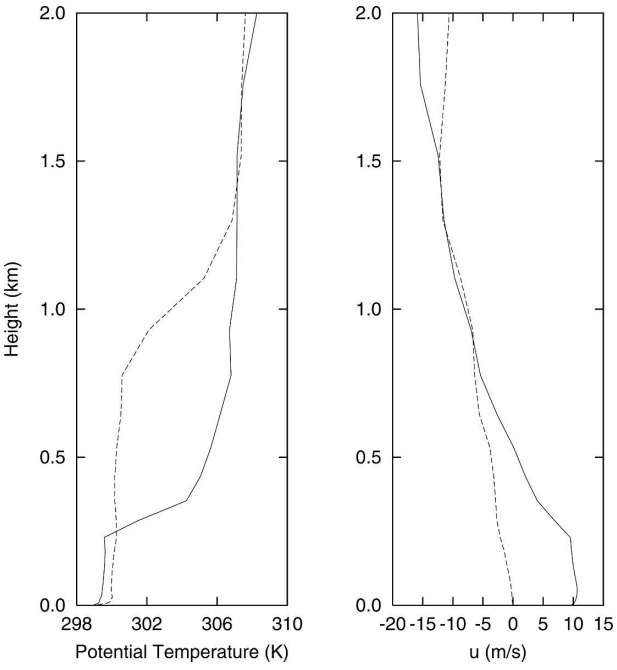

FIG. 13. Vertical profiles of potential temperature and zonal velocity in the model approximately 50 km west of Weipa for the 18 October NACL case at 1800 (solid line) and 0000 EST (dashed line) half an hour prior to the passage of the developing NACL.

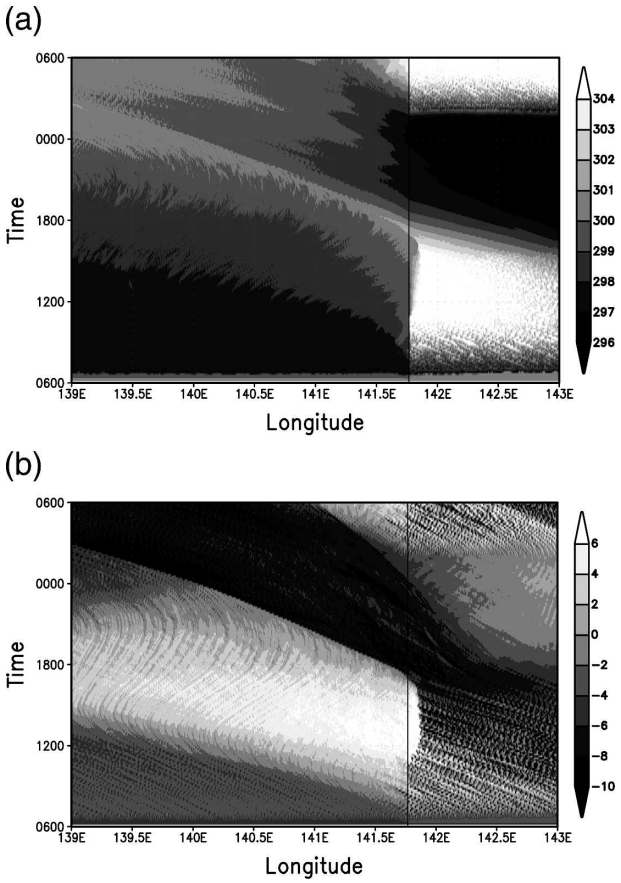

FIG. 14. Hovmöller plots of (a) potential temperature and (b) zonal velocity in the numerical model at ground level for the 20 October NACL case. The vertical line marks the position of the west coast.

easterly flow in the Hovmöller plot of zonal wind shown in Fig. 14b. It is the convergence at the leading edge of this land breeze that leads to upward motion producing the NACL.

The formation of the NACL described here is different from the formation of the northeasterly morning glory described in Goler and Reeder (2004). Morning glories form farther south when the east and west coast sea breezes meet. As Cape York Peninsula becomes wider to the south, the sea breezes meet much later at about 2200 EST. In this case, the more buoyant east coast sea breeze overrides the west coast sea breeze and, in the process, generates a series of small amplitude waves on the west coast sea breeze. These waves resonantly amplify, if they propagate at approximately the same speed as the east coast sea breeze, as they remain stationary relative to its leading edge. Through nonlinear effects, the wave speed increases with increasing amplitude and the waves propagate ahead of the east coast sea breeze to form the morning glory. By the time this occurs, the leading edge of the east coast sea breeze is some 100 km west of the leading edge of the west coast sea breeze. The demise of the west coast sea breeze, which occurs after the morning glory has developed, plays no role in the formation of the morning glory since the morning glory develops at the leading edge of the east coast sea breeze.

6. Conclusions

Aircraft measurements of the two most prominent NACL events out of four documented during GLEX have been presented, together with measurements of the sea-breeze environment over Cape York Peninsula prior to the formation of the NACL. Unlike the NACLs observed during AMEX, the events during GLEX formed just after local midnight and were not preceded by deep convection. Moreover, the NACLs during GLEX were much shallower than those during AMEX, the cloud depths being less than 1 km deep and precipitation was absent.

The generation of the NACL is linked to the sea breezes that develop over the peninsula on the previous day. For this reason, the experiment documented the sea-breeze structure as the east coast and west coast sea breezes interacted near the west coast of Cape York Peninsula, with the observations from one particular aircraft mission presented (7 October). The west coast

sea breeze was well defined with a very sharp leading edge but it did not penetrate far inland, as it was opposed by the low-level synoptic flow. In contrast, the east coast sea breeze was poorly defined and highly modified by daytime heating as the air crossed the peninsula.

Several research aircraft flights focused on the mature NACL structure in the early morning. Two examples of this type of mission, the events of 18 and 20 October, were described herein. The NACL was marked by a drop in potential temperature at low levels and it was shown to propagate on the leading edge of a gravity current. The zonal (or normal) near-surface wind component showed strong easterly flow behind, or east of, the NACL with much weaker easterlies ahead of it and ascent at the leading edge. Numerical model simulations of two NACL events were presented and showed that the gravity current that produces the NACL originates as a land breeze that moves westward from Cape York Peninsula as the west coast sea breeze decays. The leading edge of this land breeze is marked by a sharp increase in easterly wind. Upward motion at this leading edge due to convergence leads to the development of cloud, resulting in the NACL visible in satellite images.

Observations showed that the decay of the NACL was associated with a warming of the air behind the NACL, leading to a decrease in the low-level convergence and a weakening of the associated updraft at the leading edge. If the depth of convection of the NACL was large enough to support precipitation, cool air downdrafts developing from evaporation of rain could supply cool air behind the NACL to counter the warming from the surface. Such a process was present in the NACLs observed during the Australian Monsoon Experiment (AMEX) and would account for some of the differences with the NACLs presented here. In particular, such downdrafts can be expected to be important in the evolution of NACLs during the wet season when atmospheric instability is greater. Such situations will be the focus of a future study.

Acknowledgments. We thank the Australian Bureau of Meteorology for its support, especially the Queensland and Northern Territory Regional Offices and the Bureau of Meteorology Research Centre. We are grateful to the following participants from Monash University, University of British Columbia, Airborne Research Australia, and the University of Munich: Andrew Coutts, Rudi Gaissmaier, Thomas Hamburger, Gabriel Kalotay, Carsten Kykal, Heinz Lösslein, Andreas Ropuack, Thomas Spengler, Rosemary Seymour, Bernadett Weinzierl, Hilbert Wendt, and Hongyan Zhu. Funding for the experiment was provided by the Australian Bureau of Meteorology, the German Research Council (Deutsche Forschungsgemeinschaft), and the Monash University Small Grant Scheme.

REFERENCES

Christie, D. R., 1992: The morning glory of the Gulf of Carpentaria: A paradigm for non-linear waves in the lower atmosphere. *Aust. Meteor. Mag.,* **41,** 21–60.

Clark, T. L., 1977: A small scale numerical model using a terrain following coordinate transformation. *J. Comput. Phys.,* **24,** 186–215.

Clarke, R. H., 1984: Colliding sea-breezes and the creation of internal atmospheric internal bore waves: Two-dimensional numerical studies. *Aust. Meteor. Mag.,* **32,** 207–226.

——, 1986: Several atmospheric bores and a cold front over southern Australia. *Aust. Meteor. Mag.,* **34,** 65–76.

——, R. K. Smith, and D. G. Reid, 1981: The Morning Glory of the Gulf of Carpentaria: An atmospheric undular bore. *Mon. Wea. Rev.,* **109,** 1726–1750.

Doviak, R. J., and D. R. Christie, 1989: Thunderstorm-generated solitary waves: A wind shear hazard. *J. Aircr.,* **26,** 423–431.

Drosdowsky, W., and G. J. Holland, 1987: North Australian cloud lines. *Mon. Wea. Rev.,* **115,** 2645–2659.

——, ——, and R. K. Smith, 1989: Structure and evolution of North Australian cloud lines during AMEX Phase I. *Mon. Wea. Rev.,* **117,** 1181–1192.

Goler, R. A., 2005: The generation of cloud lines over Cape York Peninsula. Ph.D. thesis, Monash University, 210 pp.

——, and M. J. Reeder, 2004: The generation of the morning glory. *J. Atmos. Sci.,* **61,** 1360–1376.

Haase, S. P., and R. K. Smith, 1984: Morning glory wave clouds in Oklahoma: A case study. *Mon. Wea. Rev.,* **112,** 2078–2089.

Hoinka, K. P., and R. K. Smith, 1988: A dry cold front in southern Bavaria. *Weather,* **43,** 255–260.

Holland, G. J., J. L. McBride, R. K. Smith, D. Jasper, and T. Keenan, 1986: The BMRC Australian Monsoons Experiment: AMEX. *Bull. Amer. Meteor. Soc.,* **67,** 1466–1472.

Jackson, G. E., R. K. Smith, and T. Spengler, 2002: The prediction of low-level mesoscale convergence lines over northeastern Australia. *Aust. Meteor. Mag.,* **51,** 13–24.

Lilly, D. K., 1962: On the numerical simulation of buoyant convection. *Tellus,* **14,** 145–172.

Menhofer, A., R. K. Smith, M. J. Reeder, and D. R. Christie, 1997a: Morning Glory disturbances and the environment in which they propagate. *J. Atmos. Sci.,* **54,** 1712–1725.

——, ——, ——, and ——, 1997b: The bore-like character of three morning glories observed during the Central Australian Fronts Experiment. *Aust. Meteor. Mag.,* **46,** 277–285.

Moncrieff, W. M., and M. J. Miller, 1976: The dynamics and simulation of tropical cumulonimbus and squall lines. *Quart. J. Roy. Meteor. Soc.,* **102,** 373–394.

Noonan, J. A., and R. K. Smith, 1986: Sea breeze circulations over Cape York Peninsula and the generation of Gulf of Carpentaria cloud line disturbances. *J. Atmos. Sci.,* **43,** 1679–1693.

——, and ——, 1987: The generation of the North Australian cloud line and the "Morning Glory." *Aust. Meteor. Mag.,* **35,** 31–45.

Purdom, J. F. W., 1976: Some uses of high-resolution GOES imagery in the mesoscale forecasting of convection and its behavior. *Mon. Wea. Rev.,* **104,** 1474–1483.

Puri, K., G. S. Dietachmayer, G. A. Mills, N. E. Davidson, R. A. Bowen, and L. W. Logan, 1998: The new BMRC Limited Area Prediction System, LAPS. *Aust. Meteor. Mag.,* **47,** 203–223.

Reeder, M. J., and D. R. Christie, 1998: Four nonlinear wave disturbances observed simultaneously over northern Queensland, Australia. *Weather,* **53,** 134–140.

——, and R. K. Smith, 1998: Mesoscale meteorology. *Meteorology of the Southern Hemisphere,* D. Vincent and D. J. Karoly, Eds., Amer. Meteor. Soc., 201–241.

——, D. R. Christie, R. K. Smith, and R. Grimshaw, 1995: Interacting morning glories over northern Australia. *Bull. Amer. Meteor. Soc.,* **76,** 1165–1171.

Simpson, J. E., and R. E. Britter, 1980: A laboratory model of an atmospheric mesofront. *Quart. J. Roy. Meteor. Soc.,* **106,** 485–500.

Smagorinsky, J., 1963: General circulation experiments with the primitive equations. I. The basic experiment. *Mon. Wea. Rev.,* **91,** 99–164.

Smith, R. K., 1986: Evening Glory wave-cloud lines in northwestern Australia. *Aust. Meteor. Mag.,* **34,** 27–33.

——, 1988: Traveling waves and bores in the lower atmosphere: The "Morning Glory" and related phenomena. *Earth-Sci. Rev.,* **25,** 267–290.

——, and J. Goodfield, 1981: The Morning Glory expedition. *Weather,* **36,** 130–136.

——, and B. R. Morton, 1984: An observational study of northeasterly "Morning glory" wind surges. *Aust. Meteor. Mag.,* **33,** 51–63.

——, and M. A. Page, 1985: "Morning glory" wind surges and the Gulf of Carpentaria cloud line of 25–26 October 1984. *Aust. Meteor. Mag.,* **33,** 185–194.

——, and J. A. Noonan, 1998: On the generation of low-level mesoscale convergence lines over northeastern Australia. *Mon. Wea. Rev.,* **126,** 167–185.

——, N. Crook, and G. Roff, 1982: The Morning Glory: An extraordinary atmospheric undular bore. *Quart. J. Roy. Meteor. Soc.,* **108,** 937–956.

——, M. J. Coughlan, and J. Evans-Lopez, 1986: Southerly nocturnal wind surges and bores in northeastern Australia. *Mon. Wea. Rev.,* **114,** 1501–1518.

——, M. J. Reeder, P. May, and H. Richter, 2006: Low-level convergence lines over northeastern Australia. Part II: Southerly disturbances. *Mon. Wea. Rev.,* **134,** 3109–3124.

Tapper, N. J., 1988: Surface energy balance studies in Australia's seasonally wet tropics: Results from AMEX Phase I and II. *Aust. Meteor. Mag.,* **36,** 61–68.

Thomsen, G., and R. K. Smith, 2006: Simulations of low-level convergence lines over northeastern Australia. *Quart. J. Roy. Meteor. Soc.,* **132,** 691–707.